

Mechanical properties of nanosheets and nanotubes using a new geometry independent volume definition

Philipp Wagner¹, Viktoria V. Ivanovskaya¹, Mark J. Rayson²,
Patrick R. Briddon³, Christopher P. Ewels¹

¹Institut des Matériaux Jean Rouxel (IMN), Université de Nantes, CNRS UMR 6502, 44322 Nantes, France

²Dept. Eng. Sciences and Mathematics, Luleå University of Technology, 97187 Luleå, Sweden

³School of Electrical and Electronic Engineering, University of Newcastle, Newcastle upon Tyne, NE 1 7RU, United Kingdom

E-mail: philipp.wagner@cnrs-imn.fr, chris.ewels@cnrs-imn.fr

Abstract. Cross-sectional area and volume become difficult to define as material dimensions approach the atomic scale. This limits transferability of macroscopic concepts such as Young's modulus. We propose a new volume definition where the enclosed nanosheet or nanotube average electron density matches that of the parent layered bulk material. We calculate Young's moduli for various nanosheets (including graphene, BN and MoS₂) and nanotubes. Further implications of this new volume definition such as Fermi level dependent Young's modulus and out-of-plane Poisson's ratio are shown.

See also *J. Phys.: Condens. Matter* 25, (15) 155302, 2013

1. Introduction

While mechanical reinforcement with single-wall carbon nanotubes (SWCNTs) has been a hot topic since the 1990s [1], recently interest is also growing in individual-layer or few-layer based nanomaterials such as graphene, BN and MoS₂ [2, 3, 4, 5]. Bulk mechanical properties are commonly specified using well defined parameters such as Young’s modulus E (see also [1] and [6]). When making the transition to nanoobjects this leads to complications, since the object boundaries and hence volume and cross-section have no general and transferable definition. Thus while elastic tensors remain unambiguously defined at these scales, the conversion of both experimental and theoretical strains and forces into mechanical constants such as Young’s modulus require a definition of mechanically active volume.

To date no such generalised and transferable volume definition exists. A common approach is to use geometric “macroscopic” volume models such as a rectangular slab for flat graphene or an empty cylinder for SWCNTs. However literature values chosen for the thickness t of the graphene slab or SWCNT cylinder range from $t = 0.6 - 3.4$ Å [7, 8], leading to wildly different volumes or cross-sections. The result is a wide scatter in reported values of the in-plane Young’s modulus for graphene and the axial Young’s modulus for SWCNTs, between $0.5 - 5.0$ TPa [7, 8]. Currently the most common approach for graphene is to consider it as a uniform slab with thickness of the interlayer spacing of graphite (3.35 Å). When both theory and experiment adopt this same value, the result is reasonably matching values of the in-plane Young’s modulus between theory 0.86 [9] - 1.11 TPa [10] and experiment 1.0 [11] - 1.02 TPa [12]. Simply transferring the graphite inter-layer distance to the cylinder thickness for SWCNTs provokes questions about the influence of curvature on the volume [13, 14], especially for narrow nanotubes. To date all such geometric approaches have in common the lack of a conceptual framework required for its generalisation to other related structures.

Volume can alternatively be defined based on a sum of spherical overlapping atomic radii, such as covalent or Van der Waals radii [15, 16, 17, 18]. However by drawing on a library of pre-existing small molecules rather than considering the precise system in hand, such definitions once again suffer from a lack in transferability. Notably π -bond systems are very poorly represented via Van der Waals radii [19]. Thus to date there is no general method to describe mechanically active nanoobject volume, capable of describing different kinds of structures without introducing various empirical or experimental parameters.

In this article we present a new geometry independent, parameter free and transferable volume definition based on the electron density distribution in the material, accessible from general density functional (DFT) calculations. We apply this to calculations of Young’s modulus and Poisson’s ratio of nanosheets and single-wall carbon nanotubes. This new definition provides a robust, reliable, quantitative basis for future mechanical studies of nanomaterials.

2. Method

In the following study we use DFT calculations under the local density approximation, implemented in the *AIMPRO* code [20, 21, 22]. Relativistic pseudopotentials are included via the Hartwigsen-Goedecker-Hutter scheme [23]. The basis consists of Gaussian function sets multiplied by polynomial functions including all angular momenta up to maxima p ($l = 0, 1$) and d ($l = 0, 1, 2$) [24]. For example, for carbon a *pddd* basis set was used, resulting in 38 independent functions. Periodic boundary conditions are used, with system-dependent plane wave energy cutoffs up to 175 Ha (Ha: Hartree energy), and a non-zero electron temperature of $kT = 0.04$ eV to create electronic level occupation. The k -point grids were sufficiently fine to give energies converged to better than 10^{-7} Ha. Atomic positions and lattice parameters were geometrically optimised until the maximum atomic position change in a given iteration dropped below 10^{-6} a_0 (a_0 : Bohr radius). To avoid interaction, supercell sizes were chosen such that the distance between structures was larger than 22.7 a_0 (12 Å). For Young's modulus calculations we apply small strains ϵ ($\pm 0.5, \pm 1.0, \pm 2.0$ %) staying in the harmonic regime, leading to

$$E = \frac{1}{V_0} \left. \frac{\partial^2 U}{\partial \epsilon^2} \right|_{\epsilon=0}, \quad (1)$$

as an expression of the Young's modulus E . V_0 defines the volume at equilibrium and U the total energy. A detailed description of the Young's modulus calculations is given in [6].

3. Volume definition based on the electron density

In order to define nanoobject volume, we start with the average electron density ρ of a bulk material. This can always be defined as $\rho_{bulk} = Q_{total}/V_0$, where Q_{total} gives the total number of electrons in a cell of volume V_0 , *e.g.* the conventional unit cell. For any system the local electron density $n(\vec{r}_i)$ ($i = 1..N$) can be generated in real space at every point \vec{r}_i in a fine uniform 3D mesh of N points in a supercell. Many DFT codes such as *AIMPRO* already define a real-space 3D mesh to describe the system electron density, and thus for computational efficiency we use the pre-generated mesh in the following analysis. The grid mesh density is sufficiently fine that the final calculated volume is converged to less than 1% variation (see [6]).

The total number of electrons in the supercell (SC) with known volume V_{SC} is fixed, and can be expressed as the sum of the electron density over all points multiplied by the fractional volume associated with every point,

$$Q_{total} = \frac{V_{SC}}{N} \cdot \sum_{i=1}^N n(\vec{r}_i). \quad (2)$$

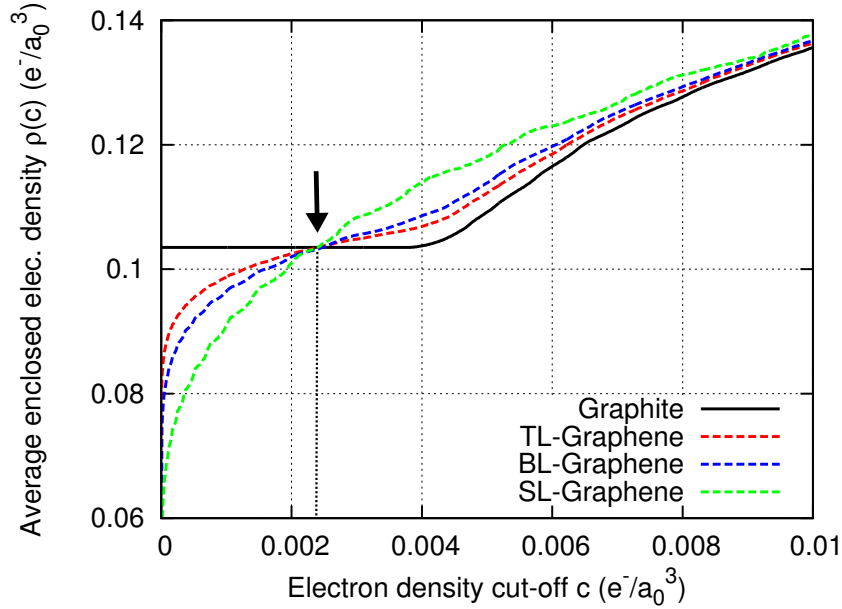


Figure 1. Average enclosed electron density $\rho(c) = Q(c)/V(c)$ as a function of the electron density cut-off c for single-layer (SL), bi-layer (BL), tri-layer (TL) graphene and graphite. The arrow indicates the cut-off given by (5), values shown in Table 1.

This definition is independent of the type of structure or supercell, for example a bulk calculation or a single-layer nanosheet surrounded by vacuum. In order to define nanoobject volume we now introduce an electron density cut-off c . We can find all the points $N_{n>c}$ with electron density $n(\vec{r}_i) > c$. This leads to the number of electrons $Q(c)$ and volume $V(c)$, knowing V_{SC} and the number of grid points N ,

$$Q(c) = \frac{V_{SC}}{N} \cdot \sum_{i=1}^{N_{n>c}} n(\vec{r}_i), \quad (3)$$

$$V(c) = \frac{N_{n>c}}{N} \cdot V_{SC}. \quad (4)$$

We propose to choose this electron density cut-off such that *the resultant nanoobject volume (here nanosheet or nanotube volume) has the same average electron density as the parent (layered) bulk material*:

$$\rho_{bulk} = \left(\frac{Q(c)}{V(c)} \right)_{nanoobject} = \rho(c)_{nanoobject}. \quad (5)$$

This leads to a new expression for the volume $V(c) = Q(c)/\rho_{bulk}$ where c corresponds to the crossing point of the average electron densities for nanosheet or nanotube and parent layered bulk material, as indicated with an arrow in Figure 4 for single- (SL), bi- (BL), tri-layer (TL) graphene with graphite. In all systems examined here these volumes enclose more than 99.35 % of the total electrons in the supercell (see Table 1

and 5 and [6]). The Young's modulus E can now be expressed using volume $V_0(c)$, which is only dependent on the electron distribution and thus takes directly into account the geometry of the structure,

$$E(c) = \frac{1}{V_0(c)} \left. \frac{\partial^2 U}{\partial \epsilon^2} \right|_{\epsilon=0}. \quad (6)$$

4. Young's modulus of nanosheets and nanotubes

Calculated Young's moduli using the new volume definition for single-, bi- and tri-layer graphene are in good agreement with experimental values of ≈ 1 TPa [12] (see Table 1). Since these experimental values assume slabs with graphite inter-layer thickness of 3.35 Å, we converted our volumes into equivalent slab thicknesses for comparison. Although we note that the enclosed volumes are in reality not uniform slabs but show surface undulation reflecting the electron distribution in the underlying lattice. The equivalent layer thickness we obtain varies with the number of layers, from 3.31 Å for SL-graphene converging towards our calculated graphite layer spacing of 3.32(3) Å with increasing layer number. This slightly smaller inter-layer distance for graphite results from the chosen pseudo-potentials and the LDA-DFT approach.

We have further calculated the Young's modulus of recently isolated nanosheets [3] using the new volume definition (Table 1). In general single-layer average thicknesses are only slightly smaller than the bulk inter-layer distance, due to the absence of extremely weak inter-layer electron delocalization effects [25]. We obtain good agreement for MoS₂ with experiment, the only one of these to be experimentally determined to date to the best of our knowledge (0.27 ± 0.1 TPa [26], 0.33 ± 0.07 TPa [27] compared to our value of 0.222 TPa).

In general the in-plane Young's moduli for nanosheets are similar to their parent bulk material: the in-plane force constants are similar, the out-of-plane interactions are weak, and the single-layer volume is close to that of one bulk layer. This observation makes prediction of nanosheet mechanical properties easier when the Young's modulus of the bulk materials are known.

Since our calculated averaged graphene layer thickness is close to the interlayer spacing of graphite, this suggests that a 3.35 Å thick geometric slab is a reasonable approximation to determine pristine graphene volume. However there are many situations for which the geometric slab model is no longer applicable (for example defective systems such as vacancy-containing graphene), where the new electron density based volume approach proposed here can still be applied.

Next the Young's moduli of different SWCNTs have been calculated. In the literature different methods have been applied but all have in common an estimated wall thickness. Using the new volume definition with equal average electron density $\rho(c)$ to graphite, the axial Young's moduli for a range of armchair, zigzag and chiral SWC-

Table 1. Calculated in-plane Young's modulus E for different nanosheets and their parent bulk materials. t indicates the single-layer thickness of a slab with equivalent volume to that defined by the electron density cut-off c . $N_Q = Q(c)/Q_{total}$ gives the ratio of enclosed electrons compared to the total number of electrons in the supercell.

Sheets	$E(c)$ (TPa)	c (e^-/a_0^3)	t (Å)	N_Q (%)
SL-Graphene	1.059	0.00240	3.31	99.64
BL-Graphene	1.059	0.00247	3.32	99.81
TL-Graphene	1.058	0.00237	3.32	99.88
4L-Graphene	1.055	0.00226	3.32	99.91
Graphite (bulk)	1.055	-	3.32	100.0
SL-BN	0.898	0.00268	3.19	99.60
BL-BN	0.891	0.00288	3.19	99.78
TL-BN	0.886	0.00277	3.19	99.86
h-BN (bulk)	0.880	-	3.19	100.0
SL-WS ₂	0.251	0.00290	6.14	99.89
WS ₂ (bulk)	0.242	-	6.17	100.0
SL-MoS ₂	0.222	0.00293	6.12	99.85
MoS ₂ (bulk)	0.219	-	6.14	100.0
SL-MoSe ₂	0.188	0.00335	6.35	99.87
MoSe ₂ (bulk)	0.188	-	6.36	100.0
SL-MoTe ₂	0.132	0.00329	6.87	99.87
MoTe ₂ (bulk)	0.132	-	6.91	100.0

NTs are summarized in Table 5 (for detailed comparison with other theoretical studies see [6]). The in-plane Young's moduli converge to that of graphite and graphene for larger diameters, and thus lower curvature. The enclosed electron ratio N_Q similarly converges to the graphene value. However the equivalent wall thickness now varies, and in particular for CNTs with diameters below around 4.7 Å the CNTs are completely filled (independent of the chirality) [6]. This agrees with the lower diameter limit for the filling of SWCNTs with water [30].

Table 2. Axial Young's modulus E calculated for different SWCNTs. t indicates the hypothetical cylinder thickness (brackets indicate completely filled tubes) centred around the SWCNT atom positions, with equivalent volume to that defined by the electron density cut-off c . $N_Q = Q(c)/Q_{total}$ gives the ratio of enclosed electrons and c the evaluated electron density cut-off.

	SWCNT	$E(c)$ (TPa)	c ($e^-/\text{\AA}^3$)	t (\AA)	N_Q (%)
(armchair)	(2,2)	0.642	0.00272	(3.04)	99.45
	(3,3)	1.049	0.00255	(3.21)	99.60
	(4,4)	0.995	0.00246	3.25	99.61
	(5,5)	1.018	0.00243	3.27	99.62
	(8,8)	1.057	0.00240	3.30	99.63
	(10,10)	1.063	0.00238	3.31	99.64
(zigzag)	(3,0)	0.885	0.00295	(3.00)	99.36
	(4,0)	0.969	0.00255	(3.12)	99.53
	(5,0)	0.969	0.00252	(3.20)	99.61
	(6,0)	1.010	0.00247	3.23	99.61
	(9,0)	1.005	0.00240	3.29	99.63
	(12,0)	1.028	0.00240	3.30	99.63
	(17,0)	1.054	0.00236	3.31	99.64
(chiral)	(4,1)	1.001	0.00244	(3.17)	99.60
	(8,2)	1.019	0.00241	3.27	99.63
	(8,4)	1.046	0.00240	3.29	99.63
	(12,6)	1.054	0.00239	3.30	99.63
Exp. E		≈ 1 TPa [28, 29]			

5. Fermi level dependent Young's modulus and Poisson's ratio of graphene

Defining volume via a well-defined cut-off in the system electron density has further conceptual implications. For example, varying the Fermi level can change the Young's modulus by depopulating bonding states or populating anti-bonding states, softening the bond spring constants of the system and hence the $\partial^2 U / \partial \epsilon^2$ term of (6). However since volume is now defined in terms of a cut-off defined for the system electron density in equilibrium, the enclosed volume will now also be Fermi level dependent. This means that changes in $1/V_0(c)$ in (6) can also modify the Young's modulus. The current approach includes both of these effects for the first time in the literature. Figure 2 shows the calculated effect of varying the Fermi level on the Young's modulus of graphene. Over moderate doping levels ($\pm 0.0625 e^-/\text{atom}$), a classical fixed volume model would suggest a gradual drop in Young's modulus as the system becomes more

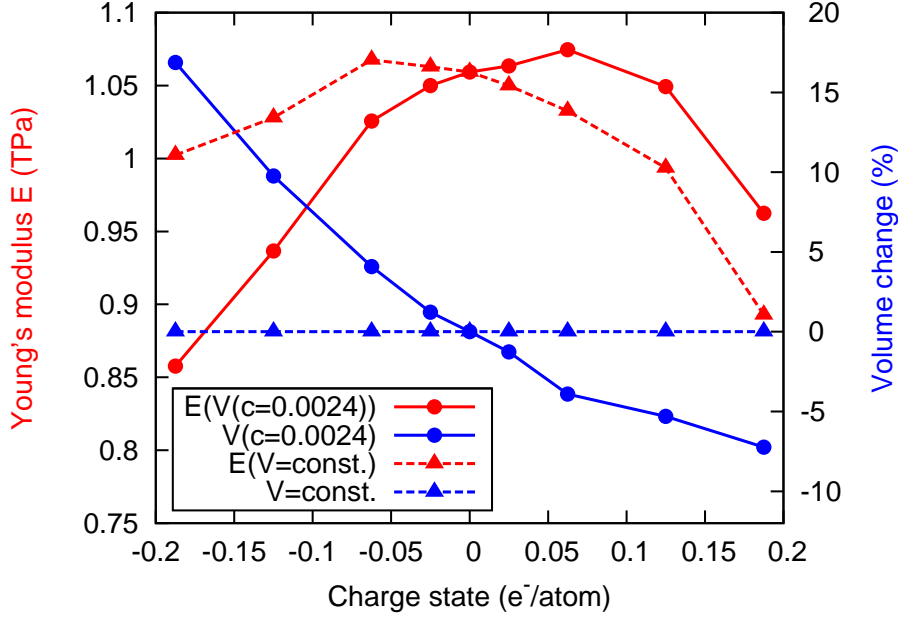


Figure 2. Young’s modulus $E(V(c=0.0024))$ and volume $V(c=0.0024)$ for graphene as a function of doping level/charge state, with volume defined using the graphene electron density cut-off of $c=0.0024 \text{ e}^-/\text{a}_0^3$. The effective Young’s modulus $E(V=\text{const.})$ fixing the volume at the charge neutral value shows the modulus variation with charge state due purely to changes in bond strength.

positive ($E(V=\text{const.})$). However this modulus trend is actually inverted once the corresponding volume decrease is included. Such complex doping-dependence of mechanical properties is not accessible with classical geometrical slab or sphere volume models.

This new volume definition also enables access to other mechanical properties such as the out-of-plane Poisson’s ratio for surface dominated nanoobjects, since it is possible to calculate the volume and hence an equivalent thickness change as the sample is strained. The Poisson’s ratio is constant for small strains, and we have taken the average for six strained/compressed cases (see [6]). For graphene we find the in-plane Poisson’s ratio to be $\nu_{12} = 0.20$ and for the first time we also calculate the out-of-plane value to be $\nu_{13} = 0.015$, using the graphene electron density cut-off $c=0.0024 \text{ e}^-/\text{a}_0^3$ [6]. Our calculated Poisson’s ratios for graphite ($\nu_{12} = 0.21$, $\nu_{13} = 0.00$) and ν_{12} for graphene are in good agreement with literature values [8].

We note that for carbon based “all surface” systems such as single-layer graphene or SWCNTs an electron density cut-off around $0.0024 \text{ e}^-/\text{a}_0^3$ delivers an accurate mechanical volume description with a very stable and very high ratio of enclosed electrons of more than 99.5 % (see also [6]). To apply such a universal material cut-off value to a broader range of structures such as nanoribbons and organic molecules would significantly extend the utility of this volume definition, and will be the subject of a future publication.

6. Conclusion

To summarise, we propose a new definition of mechanically active volume applicable to nanoobjects dervied from layered bulk materials, using a volume chosen such that the average electron density of the nanoobject matches that of the parent bulk material. This definition is geometry independent, transferable, invokes no empirical parameters and can be implemented in all standard DFT approaches. It correctly extrapolates between individual nanoobjects and bulk systems. Since both experimental and theoretical derivation of Young's modulus require a volume definition, the same calculated volumes can be applied to both. Based on this one general volume definition, for the first time consistent and comparable values for Young's moduli of various new nanosheets and single-wall carbon nanotubes have been calculated. All values show good agreement with the parent bulk in-plane Young's modulus. This can be really stated for the first time, as the calculations are based on a transferable underlying method. In addition this new approach allows study of systems whose volume varies, for example by shifting the Fermi level. It can be easily applied to nanostructures containing defects such as vacancies, which will locally modify the electron density distribution and hence volume. This volume definition could also be applied in other systems where nanoscale volume is needed such as the definition of internal porosity for metal-oxide frameworks.

Acknowledgments

PW, VVI and CPE acknowledge project NANOSIM-GRAPHENE n°ANR-09-NANO-016-01 funded by the French National Agency (ANR). We thank the CCIPL and COST Project MP0901 NanoTP for support. MJR thanks the Swedish Foundation for Strategic Research for financial support. PRB thanks the CNRS for financial support.

For references, please see at the end of the document.

Supplementary materials

J. Phys.: Condens. Matter, 25 (15) 155302, 2013

Literature approaches used to calculate Young's modulus

All theoretical calculations of Young's modulus of graphene to date have either determined the force or the total system energy change, under applied strain. These have been determined using a range of different levels of theory, including density functional theory under LDA [31, 5], GGA [32] and B3LYP [33], Hartree-Fock formalism [10], tight-binding formalism [14], empirical force constant models such as REBO [34, 35] or Brenner potentials [36], and empirical lattice dynamics models [37]. Despite the variety of techniques, the calculated values when choosing the same sample slab or cylinder thickness generally fall in a similar range.

Method to calculate the Young's modulus

The Young's Modulus E is defined as stress σ over strain ϵ ,

$$E = \sigma / \epsilon . \quad (7)$$

The strain can be defined as the fractional change in length $\epsilon = \Delta l / l_0$ along the direction of the applied strain, where l_0 defines the length at equilibrium. The stress is defined as the force F per surface area A , $\sigma = F / A$. When applying a strain the induced change in energy $\Delta U(\epsilon)$ can be expressed in terms of the total energy $U(\epsilon)$ and the equilibrium total energy $U(0)$ of the system. Using the first derivative of the energy we can write the force as

$$F = -\frac{\partial U(\epsilon)}{\partial l} = -\frac{\partial U(\epsilon)}{\partial l} \frac{\partial l}{\partial \epsilon l_0} = -\frac{\partial U(\epsilon)}{\partial \epsilon l_0} . \quad (8)$$

$U(\epsilon)$ can be expanded in the form of a n th order polynomial,

$$U(\epsilon) = a\epsilon + b\epsilon^2 + c\epsilon^3 + \dots + C . \quad (9)$$

For small strains (typically $< 5\%$) we are in the harmonic regime and $U(\epsilon)$ can be simplified to a quadratic function ($a, c, \dots \approx 0$). An example is given in Figure 3, where the energy difference $\Delta U(\epsilon)$ (10) of in-plane strained graphene with a quadratic fit is shown.

$$\begin{aligned} \Delta U(\epsilon) &= U(\epsilon) - U(0) \\ &= a\epsilon + b\epsilon^2 + c\epsilon^3 + \dots \approx b\epsilon^2 . \end{aligned} \quad (10)$$

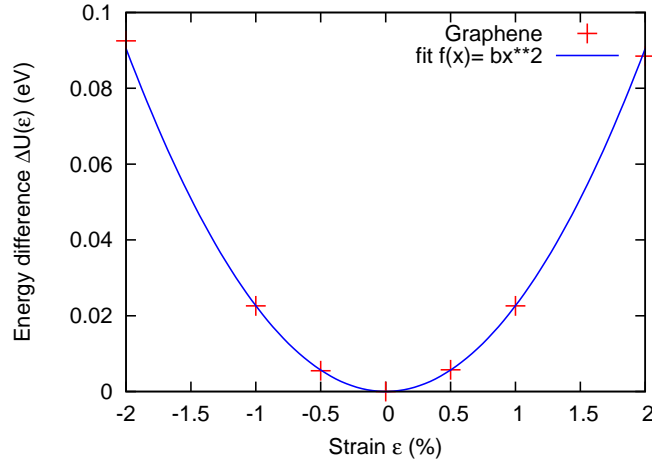


Figure 3. Total energy change for graphene (supercell with 8 carbon atoms) as a function of applied strain, with an associated quadratic fit.

The Young's modulus E can now be written in a more accessible form using (1), (2), (3) and (4),

$$E = \frac{F}{A_0 \epsilon} = \frac{\partial U(\epsilon)}{\partial \epsilon} \frac{1}{l_0 A_0 \epsilon} = \frac{2b\epsilon}{l_0 A_0 \epsilon} = \frac{2b}{V_0} \quad (11)$$

where V_0 defines the equilibrium volume. Alternatively, instead of a polynomial expansion, $U(\epsilon)$ can be developed as a Taylor Series [33]

$$U(\epsilon) = \left. \frac{\partial U}{\partial \epsilon} \right|_{\epsilon=0} \epsilon + \frac{1}{2} \left. \frac{\partial^2 U}{\partial \epsilon^2} \right|_{\epsilon=0} \epsilon^2 + \frac{1}{6} \left. \frac{\partial^3 U}{\partial \epsilon^3} \right|_{\epsilon=0} \epsilon^3 + \dots \quad (12)$$

The two approaches are equivalent and the Young's modulus in the regime of small deformations can finally be written in the form of (13), including the second derivative of the energy and the volume V_0 .

$$E = \frac{1}{V_0} \left. \frac{\partial^2 U}{\partial \epsilon^2} \right|_{\epsilon=0} = \frac{2b}{V_0}. \quad (13)$$

This approach has been used successfully by other groups [33, 36, 14] and is the basis for the Young's modulus calculations presented here.

Pure bulk (in-plane) Young's moduli have been calculated for different layered materials, shown in Table 3. To obtain the energy curve the structures were relaxed at $\epsilon = \pm 0.5, \pm 1, \pm 2$ % fixed strain along the [100] direction (in the basal planes). In these cases the bulk volume V_0 is clearly defined by the dimension of the supercell (SC) used (i.e. $V_0 = V_{SC}$). These calculations do not rely on any nanoobject volume definition but use instead well-defined bulk volumes, and can therefore be used to validate the DFT *AIMPRO* approach utilised. The agreement between our results and literature show that our potential energy curves are accurately calculated and the error from using a harmonic fit is negligible (in general less than ± 3 %).

Table 3. Calculated (in-plane) Young's modulus $E_{(100)}$ and average electron density ρ_{bulk} for different layered bulk materials. For comparison some literature values have been recalculated (marked with *) from the given elastic coefficients using $E_{(100)} = \frac{1}{s_{11}} = \frac{(c_{11}+2c_{12})(c_{11}-c_{12})}{c_{11}+c_{12}}$.

Bulk Material	This work E (TPa) ρ_{bulk} (e^-/a_0^3)	Theory E (TPa)	Experiment E (TPa)
Graphite	1.055 0.104	1.041*[38] 1.029*[40]	1.060 [39] 1.02±0.03[41]
h-BN	0.880 0.104	0.900*[42] 0.810 [40]	0.753*[43] 0.700*[44]
WS ₂	0.242 0.296	0.238*[45]	0.150 [46]
MoS ₂	0.219 0.206	0.202*[45]	0.238 [47]
MoSe ₂	0.188 0.278	0.178*[45]	-
MoTe ₂	0.132 0.295	0.124*[45]	-

These results are in general in very good agreement with the literature, although some small differences between theoretical and experimental values are to be expected. This is firstly due to the LDA-DFT approach, where bonding tends in general to be overestimated, which can lead to slightly higher in-plane forces and thus lead to slightly higher values for the Young's moduli. Secondly the experimental values can be influenced by factors such as sample purity, internal defects and grain size (for example in [44] the BN sample is pyrolytic). Additionally the measurements are often indirect (e.g. the BN values are taken from thermal conductivity studies [44] and x-ray scattering measurements [43]). Thus a difference of up to ~ 20 % between the theoretical and experimental values seems not unreasonable.

Defining the volume based on the average electron density

The variation of the ratio of enclosed electrons $N_Q(c)$ (14) and Volume $V(c)$ (15) with electron density cut-off c is shown in Figure 4(a) and (b), for single- (SL), bi- (BL), tri-layer (TL) graphene and graphite.

$$N_Q(c) = Q(c)/Q_{total} = \frac{V_{SC}}{N} \cdot \sum_{i=1}^{N_{n>c}} n(\vec{r}_i)/Q_{total} , \quad (14)$$

$$V(c) = \frac{N_{n>c}}{N} \cdot V_{SC} . \quad (15)$$

For graphite a cut-off of $c = 0.0038 \text{ e}^-/a_0^3$ already includes all points in the cell (see Figure 4(c)), and hence for cut-offs less than this there is no change in included volume or electrons. In contrast, for graphene the volume $V(c)$ increases rapidly as the cut-off drops, which can be understood as the surface charge smears out from the graphene into

the vacuum around it. Even grid points with $n(\vec{r})$ close to zero can be found. However this smeared out charge represents only a very small fraction of the total number of electrons (see Figure 4 (a)). For example at the minimal graphite cut-off of $c = 0.0038 \text{ e}^-/\text{a}_0^3$, already more than 99 % of the total number of electrons per atom in graphene are included. In general the enclosed volume is relatively insensitive to the precise cut-off value, since the electron density in the region surrounding the volume cut-off drops away rapidly. For example, increasing c from our obtained graphene cut-off value of $c=0.0024 \text{ e}^-/\text{a}_0^3$ to $0.003 \text{ e}^-/\text{a}_0^3$ only decreases the enclosed volume by 4.5%, with $N_Q = 99.52 \%$ still.

Figure 4 (d) shows that the calculated nanoobject volume converges rapidly with the grid mesh used to define the electron density. The grid mesh is given by the plane wave energy cut-off in our calculations. The volume is already converged for a plane-wave cut-off of 100 Ha. In our graphene and CNT calculations a plane wave energy cut-off of 150 Ha is used. As example for SL-graphene we used a $48 \times 54 \times 180$ grid (150 Ha) in a $7.99 \times 9.23 \times 30.00 \text{ a}_0^3$ orthorhombic supercell (see Table 4 and Figure 4 (d)). For SL-graphene calculations an energetically well converged $24 \times 24 \times 1$ k-point grid has been used.

Table 4. Parameters from the nanosheet calculations (Table 1 in the article). N_{atoms} gives the number of atoms in the supercell, $V_0(c)$ the volume calculated with the given cut-off c , and a, b the relaxed in-plane orthorhombic lattice parameters in equilibrium. (In direction c there was always enough space to avoid interactions. An orthorhombic supercell has always been used.)

Sheets	N_{atoms}	$c \text{ (e}^-/\text{a}_0^3)$	$V_0(c) \text{ (a}_0^3)$	$a \text{ (a}_0)$	$b \text{ (a}_0)$
SL-Graphene	8	0.00240	461.82	7.996	9.232
BL-Graphene	16	0.00247	926.024	7.997	9.234
TL-Graphene	24	0.00237	1390.69	7.997	9.234
4L-Graphene	32	0.00226	1855.15	7.997	9.234
SL-BN	8	0.00268	461.57	8.139	9.397
BL-BN	16	0.00288	921.68	8.143	9.402
TL-BN	24	0.00277	1383.85	8.143	9.407
SL-WS ₂	12	0.00290	1426.08	10.316	11.911
SL-MoS ₂	12	0.00293	1426.08	10.338	11.938
SL-MoSe ₂	12	0.00335	1571.81	10.654	12.299
SL-MoTe ₂	12	0.00329	1962.38	11.451	13.207

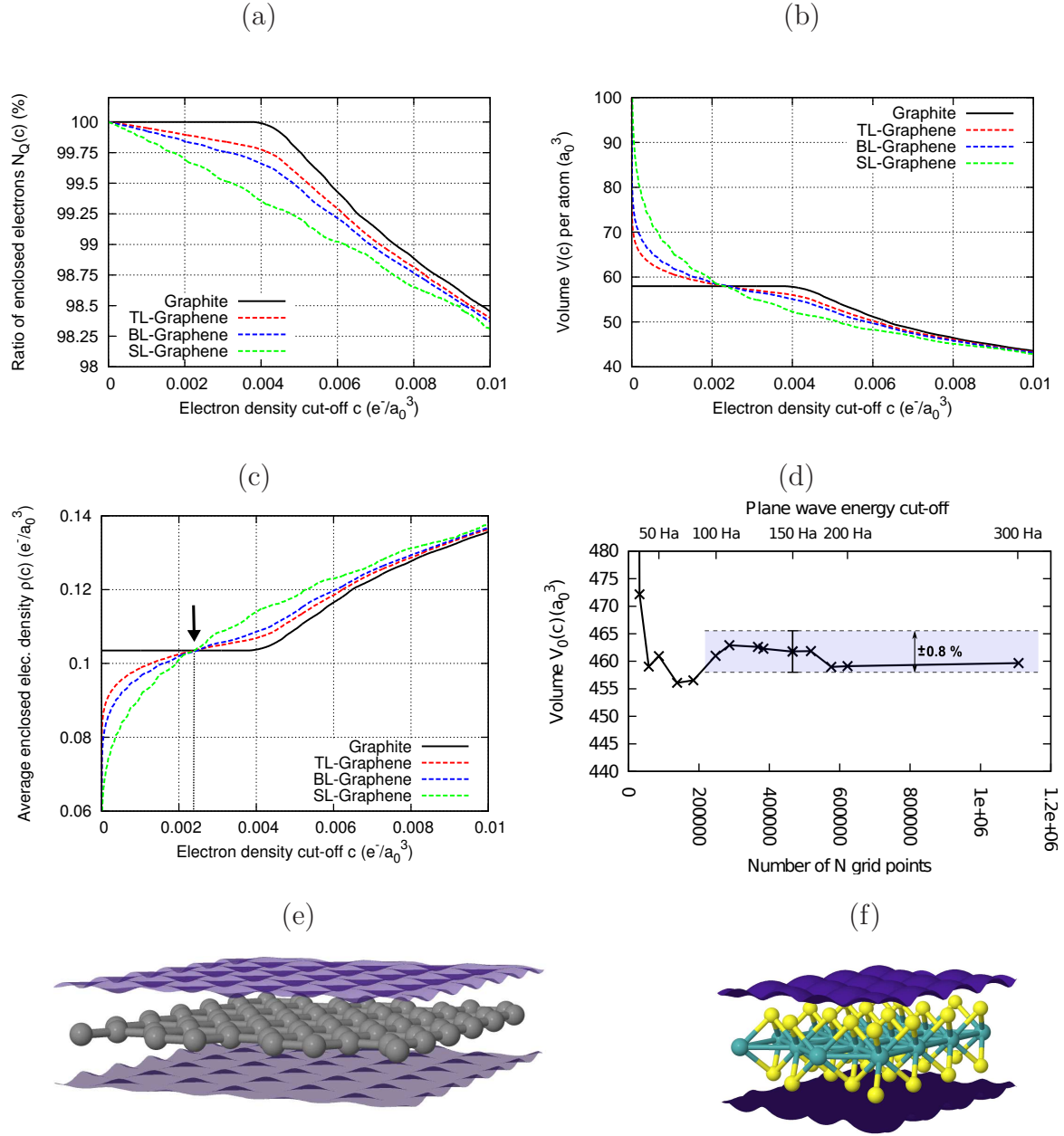


Figure 4. Variation of ratio of enclosed electrons $N_Q(c)$ (a), and volume per atom $V(c)$ (b) as a function of electron density cut-off for single-layer (SL), bi-layer (BL), tri-layer (TL) graphene and graphite. (c) Shows the resultant enclosed electron density $\rho(c) = Q(c)/V(c)$. The arrow indicates the cut-off c . In (d) the variation of confined volume for SL-graphene ($c = 0.0024$ e^-/a_0^3) as a function of plane wave energy cut-off is plotted, showing that the volume is essentially converged around 100 Ha (maximum error of less than $\pm 0.8\%$ taking 150 Ha, *i.e.* 466560 grid points). Schematic perspective images of volumes, visualized using the iso-surface of the evaluated cut-off c , are shown in (e) for SL-graphene and (f) for a MoS₂ single-layer nanosheet. Atom colours, grey: C, yellow: S, cyan: Mo.

Case study SWCNTs

Initial experimental studies found axial Young's Modulus values for SWCNTs of around 1.25 TPa, although more recent studies have found values closer to 1 TPa. Our calculated values, along with other theoretical studies are in good agreement with this, shown in Table 5. This table also shows that Young's modulus becomes diameter independent for tube diameters larger than $\sim 4 \text{ \AA}$. Isosurfaces associated with our calculated nanoobject volume for the (3,3) and (10,10) carbon nanotubes are shown in Figure 5. In Figure 6 the average electron density $\rho(c)$ of the armchair, zigzag and chiral SWCNTs as function of the cut-off c are plotted. Additionally in Figure 6 (d) an example of a radial distribution of the grid points is given.

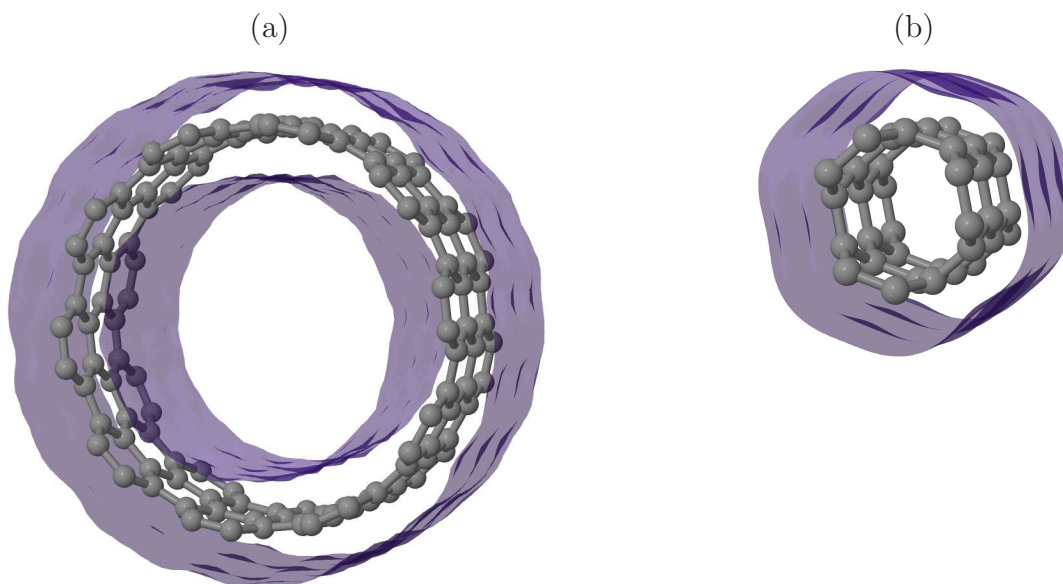


Figure 5. Schematic perspective images of CNT volumes visualized using the isosurface of the evaluated cut-off c , (a) segment of (10,10) SWCNT and (b) segment of (3,3) SWCNT (note the lack of interior cavity in (b)).

Table 5. Axial Young's modulus calculated for different SWCNTs. For the potential energy curve the SWCNTs are strained ± 0.5 , ± 1 , ± 2 % along their axis. Additionally the electron density cut-off c and the tube diameter d are indicated.

(ac: armchair, zz: zigzag, d is calculated out of 3 carbon atomic positions lying in the same plane perpendicular to the tube axis)

		This work			Theory
	SWCNT	$E(c)$ (TPa)	c (e^-/a_0^3)	d (\AA)	E (TPa)
(ac)	(2,2)	0.642	0.00272	2.79	-
	(3,3)	1.049	0.00255	4.17	-
	(4,4)	0.995	0.00246	5.48	0.96 [13]
	(5,5)	1.018	0.00243	6.82	1.11 [36]
					0.971 [34]
	(8,8)	1.057	0.00240	10.83	0.99 [13]
					0.979/1.008 [48]
	(10,10)	1.063	0.00238	13.46	1.23 [36]
					0.99 [13]
					1.24 [14]
					0.972 [34]
(zz)	(3,0)	0.885	0.00295	2.60	-
	(4,0)	0.969	0.00255	3.34	0.84 [13]
	(5,0)	0.969	0.00252	4.04	-
	(6,0)	1.010	0.00247	4.79	0.96 [13]
	(9,0)	1.005	0.00240	7.05	1.16 [36]
					0.974/1.017 [48]
	(12,0)	1.028	0.00240	9.37	-
	(17,0)	1.054	0.00236	13.20	1.227 [36]
(chiral)	(4,1)	1.001	0.00244	3.73	-
	(8,2)	1.019	0.00241	7.21	0.974 [34]
	(8,4)	1.046	0.00240	8.29	1.176 [36]
	(12,6)	1.054	0.00239	12.39	1.20 [36]
Exp. E	≈ 1 TPa [49, 28, 29, 50], 1.25 TPa [51]				

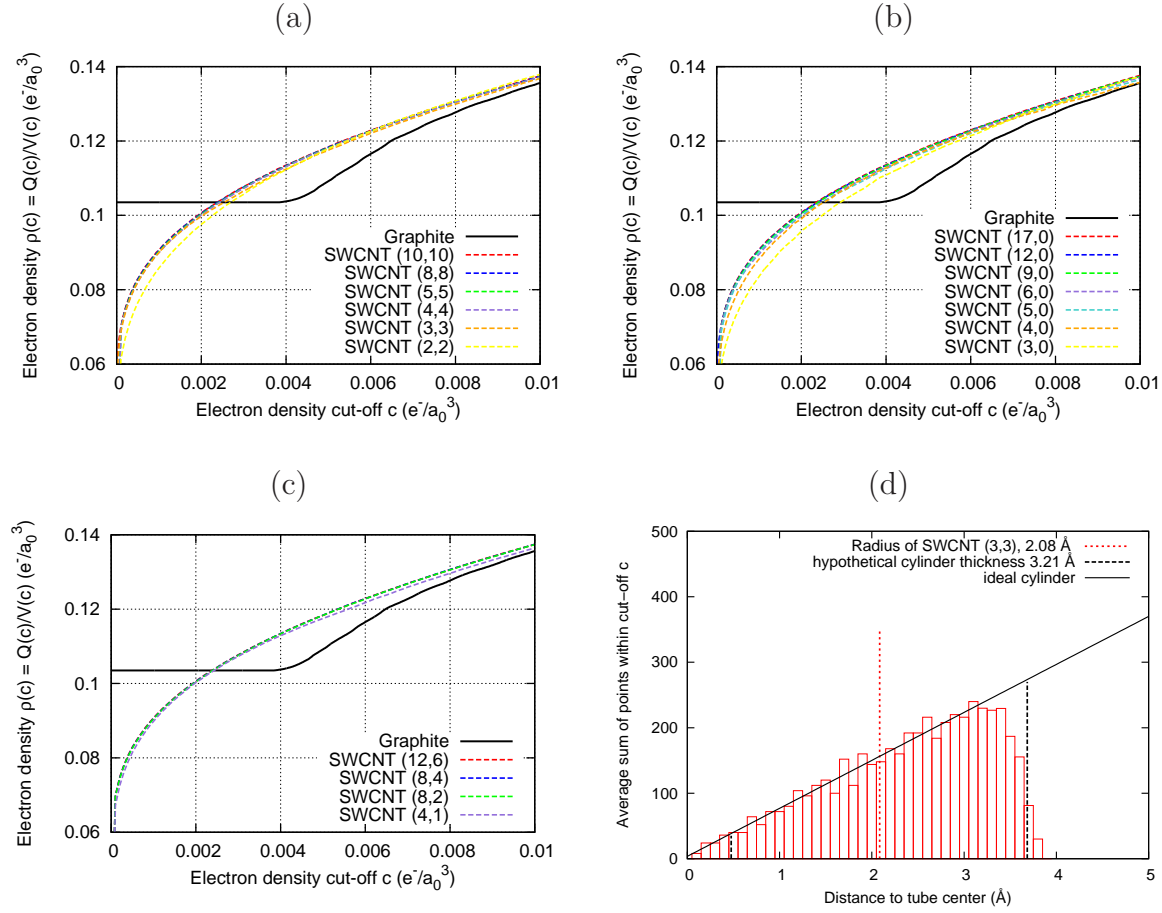


Figure 6. Comparing the average electron density $\rho(c)$ of (a) armchair SWCNTs, (b) zigzag SWCNTs and (c) chiral SWCNTs with graphite as a function of the electron density cut-off c . (d) Radial distribution of real space points within the electron density cut-off as a function of distance from the nanotube axis (averaged along tube axis, grid of 30 steps along the tube). Dotted red line marks distance of atom centres from the axis. The solid black line shows the number of points at a given radius expected for an ideal cylinder, and dotted black lines show limits of a hypothetical cylinder with inner and outer radii evenly spaced around the atom positions, with same total volume as that obtained using the electron density cut-off.

Fermi level dependent Young's modulus

Table 6 gives a detailed overview of the results obtained when changing the Fermi level / charge state of a single graphene layer. We note that the enclosed electron ratio N_Q varies very little, demonstrating the reliability of the constant-cut-off $c = 0.0024 \text{ e}^-/\text{a}_0^3$.

Table 6. Calculations of single-layer graphene. For all volumes $V(c)$ a cut-off $c = 0.0024 \text{ e}^-/\text{a}_0^3$ has been used. $N_Q = Q(c)/Q_{total}$ gives the ratio of enclosed electrons. a, b are the relaxed in-plane orthorhombic lattice parameter using a supercell with 8 carbon atoms.

charge state (e^-/atom)	$V(c) (\text{a}_0^3)$	$a (\text{a}_0)$	$b (\text{a}_0)$	$N_Q (\%)$
-0.1875	539.75	8.258	9.535	99.61
-0.125	506.87	8.143	9.403	99.61
-0.0625	480.66	8.056	9.302	99.62
-0.025	467.49	8.016	9.255	99.63
0.0	461.82	7.996	9.232	99.64
+0.025	455.95	7.985	9.219	99.65
+0.0625	443.78	7.979	9.215	99.63
+0.125	437.30	8.001	9.237	99.66
+0.1875	428.41	8.054	9.297	99.64

Poisson's ratio of graphene

When calculating the out-of-plane Poisson's ratio of graphene, the ratio of enclosed electrons N_Q remains essentially constant, while the volume increases with increasing strain (see Table 7). This again demonstrates that the cut-off obtained under equilibrium conditions is transferable. Using the same amount of enclosed electrons seems logical, as for bulk material this value also remains constant.

Table 7. Poisson's ratio calculations of single-layer graphene. For all volumes $V(c)$ a cut-off $c=0.0024 \text{ e}^-/\text{a}_0^3$ has been used. $N_Q = Q(c)/Q_{total}$ gives the ratio of enclosed electrons, t the average equivalent slab thickness. a, b are the relaxed in-plane orthorhombic lattice parameters in equilibrium using a supercell with 8 carbon atoms.

strain ϵ (%)	$V(c)$ (a_0^3)	a (a_0)	b (a_0)	t (\AA)	N_Q (%)
-2.0	454.53	7.836	9.269	3.31	99.65
-1.0	458.07	7.916	9.249	3.31	99.64
-0.5	459.96	7.956	9.241	3.31	99.64
0.0	461.86	7.996	9.231	3.31	99.64
+0.5	463.68	8.036	9.225	3.31	99.64
+1.0	465.53	8.076	9.216	3.31	99.64
+2.0	469.23	8.156	9.201	3.31	99.63

References

- [1] R. H. Baughman, A. A. Zakhidov, and W. A. de Heer. Carbon Nanotubes—the Route Toward Applications. *Science*, 297(5582):787–792, 2002.
- [2] S. Stankovich, D. A. Dikin, G. H. B. Dommett, K. M. Kohlhaas, E. J. Zimney, E. A. Stach, R. D. Piner, S. T. Nguyen, and R. S. Ruoff. Graphene-based composite materials. *Nature*, 442(7100):282–286, 2006.
- [3] J. N. Coleman, M. Lotya, A. O’Neill, S. D. Bergin, and P. J. King et. al. Two-Dimensional Nanosheets Produced by Liquid Exfoliation of Layered Materials. *Science*, 331(6017):568–571, 2011.
- [4] A. H. C. Neto and K. Novoselov. New directions in science and technology: two-dimensional crystals. *Rep. Prog. Phys.*, 74(8):082501, 2011.
- [5] P. Wagner, C. P. Ewels, V. V. Ivanovskaya, P. R. Briddon, A. Pateau, and B. Humbert. Ripple edge engineering of graphene nanoribbons. *Phys. Rev. B*, 84(13):134110, 2011.
- [6] *Supplemental materials available.*
- [7] Y. Huang, J. Wu, and K. C. Hwang. Thickness of graphene and single-wall carbon nanotubes. *Phys. Rev. B*, 74(24):245413, 2006.
- [8] F. Scarpa, S. Adhikari, and A. Srikantha Phani. Effective elastic mechanical properties of single layer graphene sheets. *Nanotechnology*, 20(6):065709, 2009.
- [9] Q. X. Pei, Y. W. Zhang, and V. B. Shenoy. A molecular dynamics study of the mechanical properties of hydrogen functionalized graphene. *Carbon*, 48(3):898–904, 2010.
- [10] G. Van Lier, C. Van Alsenoy, V. Van Doren, and P. Geerlings. Ab initio study of the elastic properties of single-walled carbon nanotubes and graphene. *Chem. Phys. Lett.*, 326(1-2):181–185, 2000.
- [11] C. Lee, X. Wei, J. W. Kysar, and J. Hone. Measurement of the Elastic Properties and Intrinsic Strength of Monolayer Graphene. *Science*, 321(5887):385–388, 2008.
- [12] C. Lee, X. Wei, Q. Li, R. Carpick, J. W. Kysar, and J. Hone. Elastic and frictional properties of graphene. *Phys. Status Solidi B*, 246(1112):2562–2567, 2009.
- [13] B. Akdim, R. Pachter, X. Duan, and W. W. Adams. Comparative theoretical study of single-wall carbon and boron-nitride nanotubes. *Phys. Rev. B*, 67(24):245404, 2003.
- [14] E. Hernández, C. Goze, P. Bernier, and A. Rubio. Elastic Properties of C and $B_xC_yN_z$ Composite Nanotubes. *Phys. Rev. Lett.*, 80(20):4502–4505, 1998.
- [15] L. Pauling. Atomic Radii and Interatomic Distances in Metals. *J. Am. Chem. Soc.*, 69(3):542–553, 1947.
- [16] P. Pyykkö and M. Atsumi. Molecular SingleBond Covalent Radii for Elements 1118. *Chem. Eur. J.*, 15(1):186–197, 2009.
- [17] A. Bondi. Van der Waals Volumes and Radii. *J. Phys. Chem.*, 68(3):441–451, 1964.
- [18] M. Mantina, A. C. Chamberlin, R. Valero, C. J. Cramer, and D. G. Truhlar. Consistent van der Waals Radii for the Whole Main Group. *J. Phys. Chem. A*, 113(19):5806–5812, 2009.
- [19] P. L. Warburton, J. L. Wang, and P. G. Mezey. On the Balance of Simplification and Reality in Molecular Modeling of the Electron Density. *J. Chem. Theory Comput.*, 4(10):1627–1636, 2008.
- [20] M. J. Rayson and P. R. Briddon. Rapid iterative method for electronic-structure eigenproblems using localised basis functions. *Comput. Phys. Commun.*, 178:128, 2008.
- [21] M. J. Rayson and P. R. Briddon. Highly efficient method for Kohn-Sham density functional calculations of 500 – 10 000 atom systems. *Phys. Rev. B*, 80(20):205104, 2009.
- [22] P. R. Briddon and M. J. Rayson. Accurate Kohn-Sham DFT with the speed of tight binding: Current techniques and future directions in materials modelling. *Phys. Status Solidi B*, 248(6):1309–1318, 2011.
- [23] C. Hartwigsen, S. Goedecker, and J. Hutter. Relativistic separable dual-space Gaussian pseudopotentials from H to Rn. *Phys. Rev. B*, 58:3641, 1998.
- [24] J. P. Goss, M. J. Shaw, and P. R. Briddon. Marker-Method Calculations for Electrical Levels

- Using Gaussian-Orbital Basis Sets. *Topics Appl. Physics*, 104:69–94, 2007.
- [25] J.-C. Charlier, X. Gonze, and J.-P. Michenaud. Graphite Interplanar Bonding: Electronic Delocalization and van der Waals Interaction. *Europhys. Lett.*, 28(6):403–408, 1994.
 - [26] S. Bertolazzi, J. Brivio, and A. Kis. Stretching and Breaking of Ultrathin MoS₂. *ACS Nano*, 5(12):9703–9709, 2011.
 - [27] A. Castellanos-Gomez, M. Poot, G. A. Steele, H. S. J van der Zant, N. Agraït, and G. Rubio-Bollinger. Elastic Properties of Freely Suspended MoS₂ Nanosheets. *Adv. Mat.*, 24:772–775, 2012.
 - [28] J.-P. Salvetat, G. A. D. Briggs, J.-M. Bonard, R. R. Bacsa, A. J. Kulik, T. Stckli, N. A. Burnham, and L. Forr. Elastic and Shear Moduli of Single-Walled Carbon Nanotube Ropes. *Phys. Rev. Lett.*, 82(5):944–947, 1999.
 - [29] M.-F. Yu, B. S. Files, S. Arepalli, and R. S. Ruoff. Tensile Loading of Ropes of Single Wall Carbon Nanotubes and their Mechanical Properties. *Phys. Rev. Lett.*, 84(24):5552–5555, 2000.
 - [30] S. Cambré, B. Schoeters, S. Luyckx, E. Goovaerts, and W. Wenseleers. Experimental Observation of Single-File Water Filling of Thin Single-Wall Carbon Nanotubes Down to Chiral Index (5,3). *Phys. Rev. Lett.*, 104(20):207401, 2010.
 - [31] F. Liu, P. Ming, and J. Li. Ab initio calculation of ideal strength and phonon instability of graphene under tension. *Phys. Rev. B*, 76(6):064120, 2007.
 - [32] R. Faccio, P. A. Denis, H. Pardo, C. Goyenola, and A. W. Mombr. Mechanical properties of graphene nanoribbons. *J. Phys.: Condens. Matter*, 21:285304, 2009.
 - [33] C. D. Zeinalipour-Yazdi and C. Christofides. Linear correlation between binding energy and Young’s modulus in graphene nanoribbons. *J. Appl. Phys.*, 106(5):054318, 2009.
 - [34] J. P. Lu. Elastic Properties of Carbon Nanotubes and Nanoropes. *Phys. Rev. Lett.*, 79(7):1297–1300, 1997.
 - [35] Y. Y. Zhang, C. M. Wang, Y. Cheng, and Y. Xiang. Mechanical properties of bilayer graphene sheets coupled by sp³ bonding. *Carbon*, 49(13):4511–4517, 2011.
 - [36] S. Gupta, K. Dharamvir, and V. K. Jindal. Elastic moduli of single-walled carbon nanotubes and their ropes. *Phys. Rev. B*, 72(16):165428, 2005.
 - [37] L. Jian Ping. Elastic properties of single and multilayered nanotubes. *J. Phys. Chem. Solids*, 58(11):1649–1652, 1997.
 - [38] Y. Qi, H. Guo, Jr. Hector, and A. Timmons. Threefold Increase in the Young’s Modulus of Graphite Negative Electrode during Lithium Intercalation. *J. Electrochem. Soc.*, 157(5):A558–A566, 2010.
 - [39] A. Kis, D. Mihailovic, M. Remskar, A. Mrzel, A. Jesih, I. Piwonski, A. J. Kulik, W. Benot, and L. Forr. Shear and Young’s Moduli of MoS₂ Nanotube Ropes. *Adv. Mat.*, 15(9):733–736, 2003.
 - [40] K. N. Kudin, G. E. Scuseria, and B. I. Yakobson. C₂F, BN, and c nanoshell elasticity from ab initio computations. *Phys. Rev. B*, 64(23):235406, 2001.
 - [41] O. L. Blakslee, D. G. Proctor, E. J. Seldin, G. B. Spence, and T. Weng. Elastic Constants of CompressionAnnealed Pyrolytic Graphite. *J. Appl. Phys.*, 41(8):3373–3382, 1970.
 - [42] N. Ohba, K. Miwa, N. Nagasako, and A. Fukumoto. First-principles study on structural, dielectric, and dynamical properties for three BN polytypes. *Phys. Rev. B*, 63(11):115207, 2001.
 - [43] A. Bosak. Elasticity of hexagonal boron nitride: Inelastic x-ray scattering measurements. *Phys. Rev. B*, 73(4):041402(R), 2006.
 - [44] L. Duclaux, B. Nysten, J.-P. Issi, and A. W. Moore. Structure and low-temperature thermal conductivity of pyrolytic boron nitride. *Phys. Rev. B*, 46(6):3362–3367, 1992.
 - [45] S. V. Khare. COLLABORATIVE RESEARCH AND DEVELOPMENT (CR&D) delivery order 0070: Ab-initio modeling of slippery hexagonal solids. Technical report, May 2008.
 - [46] C. Sourisseau, F. Cruege, M. Fouassier, and M. Alba. Second-order Raman effects, inelastic neutron scattering and lattice dynamics in 2H-WS₂. *Chem. Phys.*, 150(2):281–293, 1991.
 - [47] J. L. Feldman. Elastic constants of 2H-MoS₂ and 2H-NbSe₂ extracted from measured dispersion curves and linear compressibilities. *J. Phys. Chem. Solids*, 37(12):1141–1144, 1976.

- [48] S. Ogata and Y. Shibutani. Ideal tensile strength and band gap of single-walled carbon nanotubes. *Phys. Rev. B*, 68(16):165409, 2003.
- [49] E. W. Wong, P. E. Sheehan, and C. M. Lieber. Nanobeam Mechanics: Elasticity, Strength, and Toughness of Nanorods and Nanotubes. *Science*, 277(5334):1971–1975, 1997.
- [50] J. N. Coleman, U. Khan, W. J. Blau, and Y. K. Gun’ko. Small but strong: A review of the mechanical properties of carbon nanotube-polymer composites. *Carbon*, 44(9):1624–1652, 2006.
- [51] A. Krishnan, E. Dujardin, T. W. Ebbesen, P. N. Yianilos, and M. M. J. Treacy. Youngs modulus of single-walled nanotubes. *Phys. Rev. B*, 58(20):14013–14019, 1998.